MULTIBODY DYNAMICS 2005, ECCOMAS Thematic Conference
J.M. Goicolea, J. Cuadrado, J.C. García Orden (eds.)
Madrid, Spain, 21–24 June 2005

FLEXIBLE BODIES WITH THERMOELASTIC PROPERTIES IN MULTIBODY DYNAMICS

Andreas Heckmann*, **Martin Arnold**‡

*Vehicle System Dynamics Group
Institute of Robotics and Mechatronics, DLR German Aerospace Center
P.O. Box 1116, 82230 Wessling, Germany
e-mail: andreas.heckmann@dlr.de, web page: www.dlr.de/rm

‡ Institute of Numerical Mathematics
Department of Mathematics and Computer Science
Martin-Luther-University Halle-Wittenberg, 06099 Halle (Saale), Germany
e-mail: martin.arnold@mathematik.uni-halle.de,
web page: www.mathematik.uni-halle.de/~arnold

Keywords: thermoelasticity, flexible bodies, modal multifield approach, machine tool with thermal loads.

Abstract. *In flexible multibody dynamics elastic deformations due to thermal expansion are generally omitted since thermal displacements are usually small compared to those caused by mechanical loads. However, if a mechanical process is associated with a substantial heat generation or load, the validity of this approach has to be reviewed. In a wide range of applications such as friction brakes, thermal buckling phenomena, machine tools with thermal loads, micro-mechanical devices with resistive heating, the heat energy flow and the thermoelastic coupling cannot be ignored.*

In order to cope with those applications a consistent theoretical framework is introduced by the present paper that enables a combined thermal and elastic analysis in multibody dynamics. The theory is based on a linear material constitution that is inserted into the weak field equations of a flexible and heat conducting body.

The technical relevance of thermoelastic effects like the Gough-Joule effect, thermoelastic damping and thermally excited wave propagation is reviewed. As a consequence appropriate modelling assumptions can be deduced that enable a low-dimensional formulation of the displacement and temperature field by means of a modal multifield approach.

This approach is applied to a high-performance machine tool with thermal loads caused by linear induction drives.

1 MOTIVATION

From the thermodynamic point of view, the deformations of a flexible body in multibody simulation are usually assumed to proceed isothermally and adiabatically. Even though this concept is thermodynamic contradictory, it proved to be an adequate description for most problems in multibody dynamics.

However, if a mechanical process is associated with a remarkable heat generation or load, the validity of these premises has to be reviewed. In a wide range of applications such as friction brakes, thermal buckling phenomena, machine tools with thermal loads, micromechanical devices with resistive heating, the heat energy flow and the thermoelastic coupling cannot be ignored or are even of major concern.

Additionally the complexity of technical systems tends to increase. In order to design sophisticated systems and ensure reliable functionality, elaborate simulation environments are required. Supplementary modelling capabilities like a multifield representation enrich the application field of multibody dynamics and meet the demands of increasing complexity.

The design of high performance machine tools is an appropriate example. Working tasks in this field combine high speed motion with high demands on the accuracy. But the unavoidable losses in power transmission and the heat generation due to the working task necessarily lead to thermal loads. Industrial experience shows that beyond a specific level additional quality improvements require a combined elastic and thermal description of the system.

It is state-of-the-art to investigate the coupled thermal and thermoelastic behaviour in elaborate finite element studies. These provide high resolution results and give essential information on the design of machine components. However, the high computational effort which is necessary to evaluate these results is a drawback. It inhibits the application of the finite element method for a system dynamical analysis of the complete system. And looking one step further, a control set-up which accounts for thermally induced tool center point displacements can only be built up on an efficient multifield description.

With this background the present paper proposes a low-dimensional representation of the distributed phenomenon thermoelasticity with just a few global modes. The exposition covers theory, appropriate modelling assumptions and data provision and introduces an advanced application example.

2 THEORETICAL FRAMEWORK

2.1 Material Constitution

This paper deals with two physical fields, each specified by a pair of field variable terms. The mechanical state of a material particle is quantified by its stress tensor $\boldsymbol{\sigma}$ and its strain tensor $\boldsymbol{\varepsilon}$ and the thermal state by its temperature Θ and entropy density η.

In order to describe the properties and the influence of the material, it is presumed that the thermodynamic state of the material only depends on the current values of the field variables but not on their histories. The constitutive relation between the four field terms is supposed to define the thermodynamic state of a material point uniquely, no matter which process, which change of state variables has led to the current configuration.

Consequently it makes sense to base the material constitution on a thermodynamic potential. If strain $\boldsymbol{\varepsilon}$ and temperature Θ are chosen as independent variables, the free

energy F arises as associate function [1, Ch. 24]:

$$\mathrm{d}F = \boldsymbol{\sigma}^T \mathrm{d}\boldsymbol{\varepsilon} - \eta \mathrm{d}\Theta \,. \tag{1}$$

In praxis the introduction of a new variable ϑ, replacing the absolute temperature Θ by the increment w.r.t. the linearisation temperature Θ_0 proved to be advantageous:

$$\vartheta = \Theta - \Theta_0 \,. \tag{2}$$

The free energy, approximated by its second order Taylor expansion at a natural state, in which ϑ and $\boldsymbol{\varepsilon}$ vanish, enables the formulation of a linear constitutive equation in matrix form:

$$\begin{pmatrix} \boldsymbol{\sigma} \\ \eta \end{pmatrix} = \begin{pmatrix} \boldsymbol{H}_c & -\boldsymbol{H}_\lambda^T \\ \boldsymbol{H}_\lambda & \boldsymbol{H}_a \end{pmatrix} \begin{pmatrix} \boldsymbol{\varepsilon} \\ \vartheta \end{pmatrix} = \boldsymbol{H} \begin{pmatrix} \boldsymbol{\varepsilon} \\ \vartheta \end{pmatrix} . \tag{3}$$

The main diagonal elements of $\boldsymbol{H}$ specify the material properties of the mono-disciplinary effects. $\boldsymbol{H}_c$ can be identified as the classical 6 by 6 elasticity tensor relating stress to strain. $\boldsymbol{H}_a = \varrho c/\Theta_0$ involves the specific heat capacity c, the density ϱ and Θ_0 to relate temperature and entropy density.

If the influence of the mechanical on the thermal state, the so-called Gough-Joule effect [2], is not considered, the first row of (3) may be rewritten to extract the isotropic thermal strain $\boldsymbol{\varepsilon}_\vartheta$ [3, Vol. 1,(4.26)] (α denotes the thermal expansion coefficient):

$$\boldsymbol{\sigma} = \boldsymbol{H}_c(\boldsymbol{\varepsilon} - \boldsymbol{\varepsilon}_\vartheta) \qquad \text{with} \qquad \boldsymbol{\varepsilon}_\vartheta = \boldsymbol{H}_c^{-1}\boldsymbol{H}_\lambda^T \vartheta = (\alpha\ \alpha\ \alpha\ 0\ 0\ 0)^T \vartheta \,. \tag{4}$$

2.2 Weak Field Equations

The weak equation for the absolute position of a particle $\boldsymbol{r}(\boldsymbol{c}, t)$ as function of the Lagrange co-ordinate $\boldsymbol{c}$ and time t may be deduced from d'Alembert's principle, see e.g. [3, Vol. 2,(1.6)]:

$$\int_V [-\varrho \delta \boldsymbol{r}^T \ddot{\boldsymbol{r}} - \boldsymbol{\sigma}^T \delta\boldsymbol{\varepsilon} + \boldsymbol{f}_V^T \delta\boldsymbol{r}] \,\mathrm{d}V + \oint_B \boldsymbol{f}_B^T \delta\boldsymbol{r} \,\mathrm{d}B \;=\; 0 \,. \tag{5a}$$

$\boldsymbol{f}_V$ and $\boldsymbol{f}_B$ denote external forces acting on the volume element $\mathrm{d}V$ or boundary element $\mathrm{d}B$ respectively.

The weak equation of the temperature field results from the principle of virtual temperature [4, Sec. 7.2.1]:

$$\int_V [-(\nabla\delta\Theta)^T \boldsymbol{q} + (\Theta\dot{\eta} - S)\delta\Theta] \,\mathrm{d}V + \oint_B \boldsymbol{q}_B^T \boldsymbol{n}_B \delta\Theta \,\mathrm{d}B \;=\; 0 \,, \tag{5b}$$

where $\boldsymbol{q}$ denotes the heat flow, S symbolises the heat source density and $\boldsymbol{q}_B$ represents the heat flow at the boundary element $\mathrm{d}B$ with the outer unit normal vector $\boldsymbol{n}_B$. BIOT referred to (5b) as the complementary variational principle in heat transfer [5, Ch. 8, App. §3].

On first sight the equations (5a) and (5b) look like two un-coupled field descriptions from mono-disciplinary engineering textbooks. But the coupling becomes obvious by eliminating the dependent field variables using (3).

2.3 Modal Multifield Approach

The kinematics bases on a floating frame of reference formulation [6, Ch. 5] and gets the form:

$$\boldsymbol{r} = \boldsymbol{r}_R + \boldsymbol{c} + \boldsymbol{u} \,, \tag{6}$$

where the position vector $\boldsymbol{r}$ is decomposed into the absolute position vector of the floating frame of reference $\boldsymbol{r}_R$, the Lagrange co-ordinate of a particle $\boldsymbol{c}$ and its displacement $\boldsymbol{u}$. All vectors in (6) are resolved w.r.t. the body's frame of reference.

The displacement $\boldsymbol{u} = \boldsymbol{u}(\boldsymbol{c}, t)$ will be described with separated variables as product of time independent modal functions $\boldsymbol{\Phi}_u(\boldsymbol{c})$ and coefficients $\boldsymbol{z}_u(t)$. Within this approximation the evaluation of the strain field is feasible by means of the differential operator ∇_u [3, Vo. 1,(6.9)]:

$$\boldsymbol{u} = \boldsymbol{\Phi}_u \boldsymbol{z}_u \,, \qquad \boldsymbol{\varepsilon} = \nabla_u \boldsymbol{u} = (\nabla_u \boldsymbol{\Phi}_u)\boldsymbol{z}_u = \boldsymbol{B}_u \boldsymbol{z}_u \,. \tag{7}$$

The analogous approach is chosen for the scalar temperature field. According to Fourier's law of heat conduction [7, (1.12.16)], a ∇-operation multiplied by the thermal conductivity matrix $\boldsymbol{\Lambda}$ leads to the heat flux vector $\boldsymbol{q}$:

$$\vartheta = \boldsymbol{\Phi}_\vartheta \boldsymbol{z}_\vartheta \,, \qquad \nabla\vartheta = (\nabla \boldsymbol{\Phi}_\vartheta)\boldsymbol{z}_\vartheta = \boldsymbol{B}_\vartheta \boldsymbol{z}_\vartheta \qquad \Longrightarrow \qquad \boldsymbol{q} = -\boldsymbol{\Lambda}\boldsymbol{B}_\vartheta \boldsymbol{z}_\vartheta \,. \tag{8}$$

2.4 Equations of Motion

Now the matrices $\boldsymbol{K}_{uu}$ and $\boldsymbol{K}_{u\vartheta}$ are introduced for volume dependent integrals which can be preprocessed and accessed during the time integration of the multibody system:

$$\boldsymbol{K}_{uu} := \int_V \boldsymbol{B}_u^T \boldsymbol{H}_c \boldsymbol{B}_u \, \mathrm{d}V \,, \qquad \boldsymbol{K}_{u\vartheta} := \int_V \boldsymbol{B}_u^T \boldsymbol{H}_\lambda^T \boldsymbol{\Phi}_\vartheta \, \mathrm{d}V \,. \tag{9}$$

From the mechanical point of view the thermal field generates internal, distributed mechanical loads. Obviously there is no direct influence on the inertia properties of the body. That is why the mass, gyroscopic and centripetal terms within the equations of motion can be adopted from literature.

SHABANA in [6, (5.140)] and SCHWERTASSEK and WALLRAPP in [8, (6.308)] specified the generalised Newton-Euler equations for the unconstrained motion of a deformable body that undergoes large reference displacements.

A comparison of (5a) with these references yields the extended equations of motion:

$$\begin{pmatrix} \boldsymbol{M}_{aa} & \boldsymbol{M}_{a\alpha} & \boldsymbol{M}_{au} \\ & \boldsymbol{M}_{\alpha\alpha} & \boldsymbol{M}_{\alpha u} \\ \text{sym.} & & \boldsymbol{M}_{uu} \end{pmatrix} \begin{pmatrix} \boldsymbol{a}_R \\ \boldsymbol{\alpha}_R \\ \ddot{\boldsymbol{z}}_u \end{pmatrix} = \begin{pmatrix} \boldsymbol{h}_a \\ \boldsymbol{h}_\alpha \\ \boldsymbol{h}_u \end{pmatrix} + \begin{pmatrix} 0 \\ 0 \\ -\boldsymbol{K}_{uu}\boldsymbol{z}_u + \boldsymbol{K}_{u\vartheta}\boldsymbol{z}_\vartheta \end{pmatrix} . \tag{10}$$

The mass matrix on the left hand side of (10) is formulated as 3×3 block matrix such that the sub-matrices specify the inertia coupling between translational acceleration of the body's reference frame $\boldsymbol{a}_R$, the angular acceleration of the reference frame $\boldsymbol{\alpha}_R$ and the second time derivative of elastic co-ordinates $\ddot{\boldsymbol{z}}_u$. The right hand side terms $\boldsymbol{h}_a$, $\boldsymbol{h}_\alpha$ and $\boldsymbol{h}_u$ summarise all inertia, damping and external forces.

The added term $\boldsymbol{K}_{u\vartheta}\boldsymbol{z}_\vartheta$ represents the influence of the thermal field on the equations of motion. It may be interpreted as modal force acting on the elastic body.

Although the thermal loads do not influence the inertia quantities in (10), the displacements caused by these loads do, since the mass matrix and the vectors $\boldsymbol{h}_a$ and $\boldsymbol{h}_\alpha$ depend on the deformation state of the body.

2.5 Thermal Equation

In (5b) the natural boundary conditions are represented by the heat flux through the boundary surface. It depends on the physical circumstances how this term has to be introduced into the thermal equation. For Neumann conditions the boundary heat flux q_B is given explicitly. If convection occurs on the boundary surface a Robin or mixed boundary condition is imposed, specified by the film coefficient h_f and the bulk temperature ϑ_∞ of the fluid [7, Sec. 5.6]. Although this list is not complete, we confine ourselves to these two cases:

$$\boldsymbol{q}_B^T \boldsymbol{n}_B = -q_B - h_f(\vartheta_B - \vartheta_\infty) \,. \tag{11}$$

Besides the thermal-mechanical coupling matrix $\boldsymbol{C}_{\vartheta u} = \Theta_0 \boldsymbol{K}_{u\vartheta}^T$, the following notations are used for geometric integrals:

$$\begin{aligned} \boldsymbol{C}_{\vartheta\vartheta} &:= \int_V \Theta_0 \boldsymbol{\Phi}_\vartheta^T \boldsymbol{H}_a \boldsymbol{\Phi}_\vartheta \, \mathrm{d}V \,, \quad \boldsymbol{K}_{\vartheta R} := \oint_B h_f \boldsymbol{\Phi}_\vartheta^T \boldsymbol{\Phi}_\vartheta \, \mathrm{d}B \,, \quad \boldsymbol{Q}_{\vartheta R} := \oint_B \boldsymbol{\Phi}_\vartheta^T h_f \, \mathrm{d}B \,, \\ \boldsymbol{K}_{\vartheta\vartheta} &:= \int_V \boldsymbol{B}_\vartheta^T \boldsymbol{\Lambda} \boldsymbol{B}_\vartheta \, \mathrm{d}V \,, \qquad \boldsymbol{Q}_{\vartheta S} := \int_V \boldsymbol{\Phi}_\vartheta^T \, \mathrm{d}V \,, \qquad \boldsymbol{Q}_{\vartheta N} := \oint_B \boldsymbol{\Phi}_\vartheta^T \, \mathrm{d}B \,. \end{aligned} \tag{12}$$

Finally, the coupled, linearised thermal equation can be stated:

$$\boldsymbol{C}_{\vartheta\vartheta} \dot{\boldsymbol{z}}_\vartheta + \boldsymbol{C}_{\vartheta u} \dot{\boldsymbol{z}}_u + (\boldsymbol{K}_{\vartheta\vartheta} + \boldsymbol{K}_{\vartheta R}) \boldsymbol{z}_\vartheta = \boldsymbol{Q}_{\vartheta S} \, S_u + \boldsymbol{Q}_{\vartheta N} \, q_B + \boldsymbol{Q}_{\vartheta R} \, \vartheta_\infty \,. \tag{13}$$

The generalised velocities $\dot{\boldsymbol{z}}_u$ in (13) indicate that the temperature field depends on the displacements and the strains. Whereas the thermal effect on the displacements is well-established and widely accounted for in finite element analysis, the feedback from displacements on temperatures, called the Gough-Joule effect [2], is relatively unknown and very frequently neglected. This issue will be discussed in Sec. 3.

2.6 Multibody System Equations

Eqs. (10) and (13) are to be posted for each body of the articulated mechanism under consideration. For a global representation these equations are rewritten in condensed form for a general elastic and heat conducting body $(\;)^{(i)}$:

$$\boldsymbol{M}^{(i)} \boldsymbol{b}^{(i)} = \boldsymbol{h}_o^{(i)} + \boldsymbol{h}_m^{(i)}(\boldsymbol{z}_\vartheta^{(i)}, \boldsymbol{z}_u^{(i)}) \,, \tag{14a}$$

$$\dot{\boldsymbol{z}}_\vartheta^{(i)} = \dot{\boldsymbol{z}}_\vartheta^{(i)}(\boldsymbol{z}_\vartheta^{(i)}, \dot{\boldsymbol{z}}_u^{(i)}) \,. \tag{14b}$$

Besides the mechanical description (14a) the set-up of a thermoelastic body requires the definition of one additional, uniquely assigned element. The thermal element reflects (14b) and evaluates the thermal state of the body presuming that the thermal field of body $(\;)^{(i)}$ does not interfere with those of other bodies. If the thermal field of two bodies interact, the mutual influence has to be modelled explicitly defining appropriate boundary conditions (11). Mechanical interactions between separated bodies of a mechanism are to be modelled either as applied forces or by kinematical constraints.

The model equations of a general elastic body with thermal features have been implemented in a developer version of the industrial multibody code SIMPACK. This code uses relative joint co-ordinates to enable an efficient recursive assembly of the equations

of motion for the complete multibody system by an explicit $\mathcal{O}(N)$-formalism [9]. The relative joint co-ordinates together with the elastic co-ordinates of all bodies constitute the vector $\boldsymbol{p}$. For tree-like structures $\boldsymbol{p}$ is defined as minimum set of generalised mechanical co-ordinates.

The thermal equations of the complete system can be arranged as follows:

$$\dot{\bar{\boldsymbol{z}}}_\vartheta = \left(\dots \ \dot{\boldsymbol{z}}_\vartheta^{(i)} \ \dots \right)^T . \tag{15}$$

The pure mechanical part of the equations of motion of the complete multibody systems reads [10]:

$$\sum_{(i)} \left[\frac{\partial \boldsymbol{b}^{(i)}}{\partial \ddot{\boldsymbol{p}}} \right]^T \left[\boldsymbol{M}^{(i)} \boldsymbol{b}^{(i)} - \boldsymbol{h}_o^{(i)} - \boldsymbol{h}_m^{(i)} \right] \ = \ \bar{\boldsymbol{M}} \ddot{\boldsymbol{p}} - \bar{\boldsymbol{h}} \ = \ \boldsymbol{0} . \tag{16}$$

$\bar{\boldsymbol{M}}(\boldsymbol{p}, t)$ represents the symmetric inertia matrix of the complete multibody system. The generalised Coriolis and applied forces together with the generalised loads due to thermal influences are summarised in $\bar{\boldsymbol{h}}(\boldsymbol{p}, \dot{\boldsymbol{p}}, \bar{\boldsymbol{z}}_\vartheta, t)$.

For closed loop systems, Eqs. (16) are extended by kinematical constraints and the associated passive forces, see [6, Sec. 5.9]. Consequently the model equations of the complete system in its most general form are given by:

$$\begin{aligned} \bar{\boldsymbol{M}}(\boldsymbol{p}, t) \ddot{\boldsymbol{p}} &= \bar{\boldsymbol{h}}(\boldsymbol{p}, \dot{\boldsymbol{p}}, \bar{\boldsymbol{z}}_\vartheta, t) - \bar{\boldsymbol{G}}^T(\boldsymbol{p}, t) \boldsymbol{\lambda} , \\ \dot{\bar{\boldsymbol{z}}}_\vartheta &= \bar{\boldsymbol{c}}(\boldsymbol{p}, \dot{\boldsymbol{p}}, \bar{\boldsymbol{z}}_\vartheta, t) , \\ \boldsymbol{0} &= \bar{\boldsymbol{g}}(\boldsymbol{p}, t) \end{aligned} \tag{17}$$

with the constraint matrix $\bar{\boldsymbol{G}} := \left(\frac{\partial \bar{\boldsymbol{g}}}{\partial \boldsymbol{p}} \right) (\boldsymbol{p}, t)$ and Lagrangian multipliers $\boldsymbol{\lambda}$.

3 BASIC MODELLING ASSUMPTIONS

The theoretical framework which has been developed in Sec. 2 has led to (10) and (13), where a bi-directional coupling of the thermal and mechanical problem is given. Fortunately in most of the usual engineering applications it is possible to simplify the coupled problem. Firstly, the mechanical coupling term in the thermal equation, i.e. the Gough-Joule effect, is very frequently neglected. Secondly, it is possible to apply the so-called Duhamel assumption that states that the inertia terms associated with thermally induced displacements in the equations of motion are negligible. The following two sections are supposed to justify these simplifications.

3.1 The Coupled Thermoelastic Beam

LIFSHITZ and ROUKES [11] discussed the influence of full thermoelastic coupling on a beam structure. They considered a rectangular Euler-Bernoulli beam according to Fig. 1 with bending deflection $u(x)$ in the x-z-plane, which leads to a uni-directional strain field in x-direction $\varepsilon_{xx}(x, z)$.

The thermal description presumes linear isotropic material with thermal conductivity Λ and only accounts for thermal gradients in z-direction. Eq. (18) summarises the modelling assumptions adapting tensorial index notation, i.e. $(\ )_{,xx}$ denotes the second partial derivative w.r.t. x:

$$\vartheta_{,xx} \approx 0 , \qquad \vartheta_{,yy} = 0 , \qquad \varepsilon_{xx} = -z \, u_{,xx} , \qquad I_\vartheta = \int_A z \vartheta \, \mathrm{d}y \mathrm{d}z , \tag{18}$$

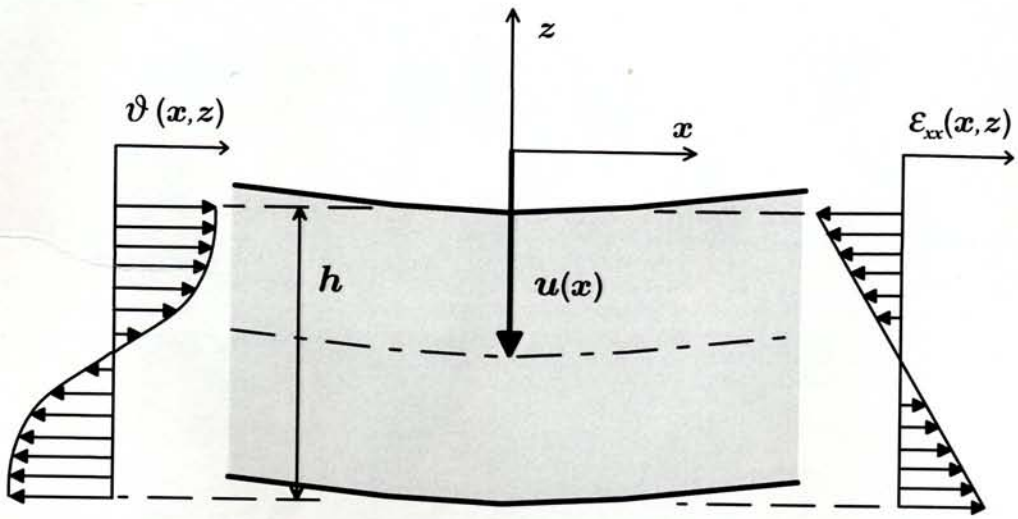

Figure 1: Co-ordinate definitions, temperature field $\vartheta(x,z)$, displacement field $u(x)$ and strain field $\varepsilon_{xx}(x,z)$ at a beam section

where the cross section integral I_ϑ represents the thermal load of the beam, see [7, (10.11.2)]. Furthermore, E denotes Young's modulus, I represents the beam's geometrical moment of inertia, h its height and A its cross section area. The coupled partial differential equations of the beam therefore get the form

$$\frac{\Lambda}{\varrho c}\,\vartheta_{,zz} + z\,E\alpha\Theta_0\,\dot{u}_{,xx} = \dot{\vartheta}\,, \tag{19a}$$

$$\varrho A\,\ddot{u} + (EI\,u_{,xx} + E\alpha I_\vartheta)_{,xx} = 0\,. \tag{19b}$$

For the solution of (19) harmonic vibrations of the beam are considered with geometrical shape functions $u_o(x)$ and $\vartheta_o(x,z)$, that align with the geometrical boundary conditions:

$$u(x,t) = u_o(x)\,\mathrm{e}^{j\omega t}\,, \qquad \vartheta(x,z,t) = \vartheta_o(x,z)\,\mathrm{e}^{j\omega t}\,, \qquad \omega \in \mathbb{C}\,. \tag{20}$$

If (20) is inserted in (19a), a particular solution of the thermal field may be obtained that satisfies the boundary condition of vanishing heat fluxes on the lateral surfaces of the beam, $\vartheta_{o,z}(z = \pm h/2) = 0$:

$$\vartheta_o = \frac{E\alpha\Theta_0}{\varrho c}\,u_{o,xx}\left[z - \frac{\sin(kz)}{k\cos(kh/2)}\right] \qquad \text{with} \qquad k = \sqrt{j\omega\frac{\varrho c}{\Lambda}}\,. \tag{21}$$

With the temperature solution (21), I_ϑ from (18) can be integrated and inserted into (19b), which yields the following eigenvalue equation:

$$\varrho A u_o\,\omega^2 - \underbrace{E\left[1 + \frac{E\alpha^2\Theta_0}{\varrho c}\left(1 + \frac{24}{h^3k^3}\left(\frac{kh}{2} - \tan\left(\frac{kh}{2}\right)\right)\right)\right]}_{\bar{E}(\omega)}\,I\,u_{o,xxxx} = 0\,. \tag{22}$$

Eq. (22) may be compared to the equation for ω_o, the eigenvalue of the corresponding classical Euler-Bernoulli beam, which may be deduced from (19b) setting the linear expansion coefficient α to 0, cf. [12, (6.120)].

It is obvious to introduce a frequency-dependent Young's modulus $\bar{E}(\omega) = E \cdot (\omega/\omega_o)^2$, which gives the following expressions in the limit cases $\mathrm{Re}\,\omega \to 0$ and $\mathrm{Re}\,\omega \to \infty$:

$$\lim_{\mathrm{Re}\,\omega \to 0} \bar{E}(\omega) = E\,, \qquad \lim_{\mathrm{Re}\,\omega \to \infty} \bar{E}(\omega) = E\left(1 + \frac{E\alpha^2\Theta_0}{\varrho c}\right)\,. \tag{23}$$

For a stiff beam with very high eigenfrequencies, the imaginary part of $\bar{E}(\omega)$ vanishes and the real part can be identified as the adiabatic Young's modulus. That means, a high frequency vibration occurs as a adiabatic process since the thermal field, which is comparable "slow" with large time constants, cannot follow the fast displacement variations.

On contrary, for weak beams with very low eigenfrequencies, $\bar{E}(\omega)$ recovers the isothermal value of Young's modulus. The displacements change very slowly, the thermal field is balanced almost all the time.

For intermediate frequencies $\bar{E}(\omega)$ and consequently ω are complex quantities. The vibration according to (20) is damped although no damping force was defined explicitly in (19b). This phenomenon is called thermoelastic damping, see [7, Ch. 2] and [1, Ch. 8].

The significance of thermoelastic damping for practical engineering problems is demonstrated in Fig. 2, which shows frequency shift s and attenuation a of a steel beam due to thermoelastic coupling. The parameter ξ combines a number of geometrical and physical parameters and is defined together with $s(\xi)$ and $a(\xi)$ as follows:

$$\xi := k_o\, h = h\sqrt{\frac{\omega_o \varrho c}{2\Lambda}}\,, \qquad a(\xi) = \frac{\mathrm{Im}\,\omega}{\omega_o}\,, \qquad s(\xi) = \frac{\mathrm{Re}\,\omega - \omega_o}{\omega_o}\,. \tag{24}$$

The attenuation reaches its maximum value $\hat{a} = 5.5 \cdot 10^{-4}$ at $\hat{\xi} = 2.23$. The maximum frequency shift is 0.1 %. The design parameter value $\hat{\xi} = 2.23$ specifies e.g. a steel beam, $h = 2\,\mathrm{mm}$ high, with the first eigenfrequency $\omega_o/(2\pi) = 4.8$ Hz (1 m long, both ends fixed).

These results clarify that for conventional structures in mechanical engineering the eigenvalues are changed only very slightly due to thermoelastic damping. From the system

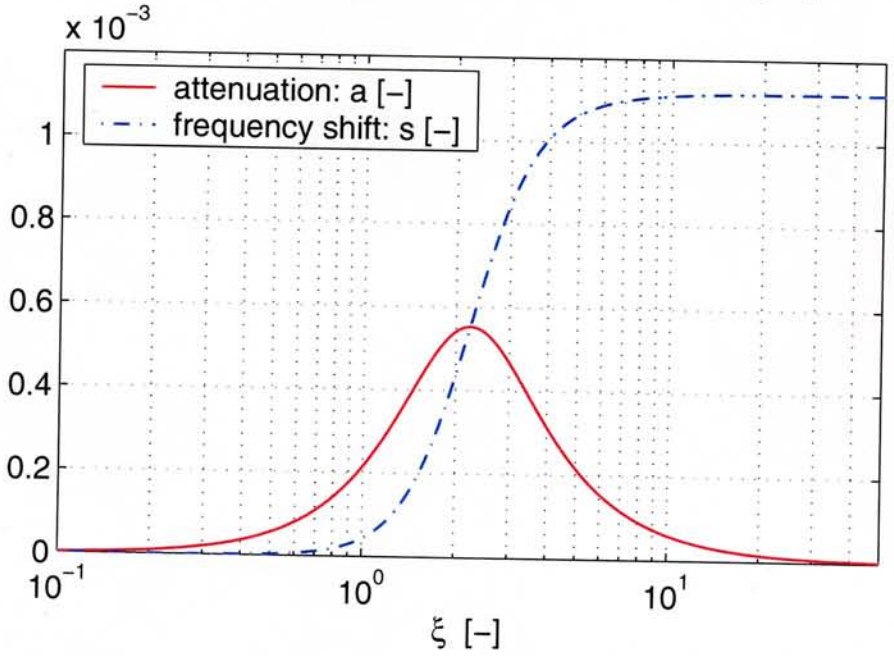

Figure 2: Attenuation and frequency shift of a rectangular steel beam due to thermoelastic coupling.

dynamical point of view the mechanical eigenvalue problem may be considered separately from the thermal eigenvalue problem. This is an important conclusion which will be exploited for the modal approach.

3.2 Duhamel's Assumption

In 1837, Duhamel noted that the mechanical inertia terms are not significant in the equations of thermoelasticity, since the time rate of temperature change is sufficiently slow (Duhamel's assumption). In 1950, this question was examined by Danilovskaya in more detail [7, Sec. 2.5]. Her argumentation supports the selection of modes which are capable to describe thermal influences on the displacement field and is therefore presented briefly in what follows.

Consider an elastic half space, $x > 0$, which is constrained in such a way that only displacements in x-direction occur. The plane $x = 0$ is suddenly exposed to a heat flux according to a Robin boundary condition with a finite film coefficient h_f. In the thermal description (19a), the mechanical coupling term is neglected. The mechanical equation is formulated in terms of stress components:

$$\frac{\Lambda}{\varrho c}\,\vartheta_{,xx} = \dot{\vartheta}\,, \tag{25a}$$

$$\frac{E(1-\nu)}{\varrho(1+\nu)\,(1-2\nu)}\,\sigma_{xx,xx} - \ddot{\sigma}_{xx} = \frac{E\alpha}{1-2\nu}\,\ddot{\vartheta}\,. \tag{25b}$$

The initial and boundary conditions are

$$\begin{aligned} \vartheta(x,0) &= 0\,, & \sigma_{xx}(x,0) &= \dot{\sigma}_{xx}(x,0) = 0\,,\\ \Lambda\,\vartheta_{,x}(0,t) &= h_f\,[\vartheta(0,t) - \vartheta_\infty\,]\,, & \sigma_{xx}(0,t) &= 0\,,\\ \lim_{x\to\infty} \vartheta(x,t) &= 0\,, & \lim_{x\to\infty} \sigma_{xx}(x,t) &= 0\,. \end{aligned} \tag{25c}$$

The analytical solution of (25) via Laplace transformation yields an expression that is somewhat cumbersome to interpret. That is why the discussion here is based on the graphical presentation of the analytical solution in Fig. 3.

It is interesting to study the behaviour for a film coefficient h_f tending towards infinity. An infinite boundary conductance means, that the boundary temperature at $x = 0$, $t = 0$ discontinuously jumps to the environmental temperature ϑ_∞ (*thermal shock load*). The structural response consists of a compressive wave propagating with sonic speed through the elastic body. Fig. 3 visualises the pressure as function of time at an exemplary point.

From a practical viewpoint it is even more interesting to study the behaviour for smaller film coefficients h_f. The maximum pressure decreases very rapidly for finite boundary conductances. Even in heat exchanger design real film coefficients beyond $10^5\,\mathrm{W/(m^2K)}$ cannot be reached.

As a consequence for real load cases the wave propagation of thermoelastic loads may be disregarded without introducing a substantial error. Since wave propagation is a genuine inertia effect it may be concluded that the inertia terms are negligible in the equations of thermoelasticity. This conjecture was considered at the very beginning when the theory of thermoelasticity was developed by Duhamel in 1837.

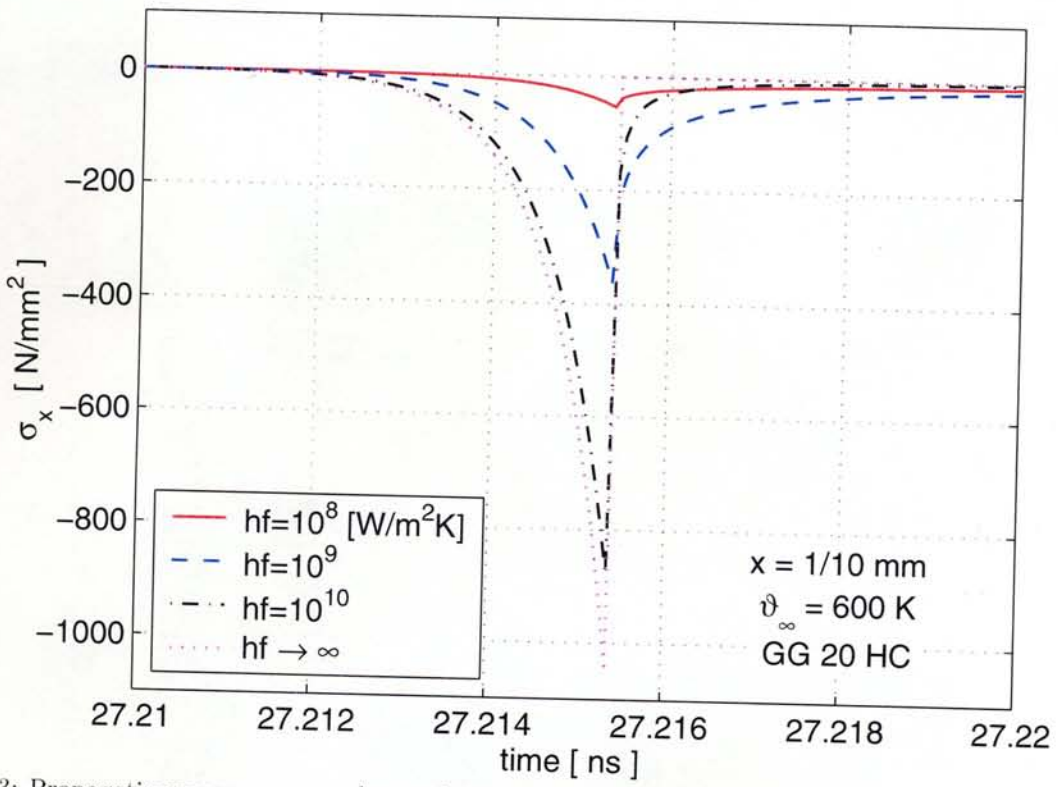

Figure 3: Propagating pressure waves due to thermal shock for various film coefficients h_f. The results are based on the analytical solution of (25), evaluated for the material GG20HC at the position $x = 1/10\,\mathrm{mm}$.

3.3 Thermal Response Modes

The just introduced analytical models motivate simplifications. Firstly they allow to deal with the thermal eigenvalue problem and the mechanical eigenvalue problem separately. Secondly they justify to neglect inertia terms regarding deflections due to thermal loads.

These considerations lead to a specific modal reduction scheme that organises the access to existing finite element data and its transfer into the modal representation. This scheme consists of four steps. In order to illustrate these reduction steps, the finite element model of a circular disc shown in Fig. 4 has been selected as sample structure.

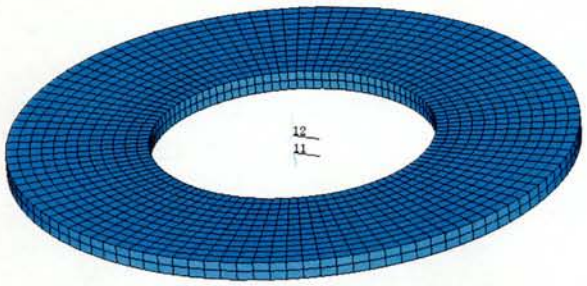

Figure 4: Finite element model illustrating the steps of the modal reduction scheme.

1. Firstly, the thermal finite element description has to be reduced. The modal approach in (7) is rewritten in discretised form for the temperature ϑ at a specific node k, located at $\boldsymbol{c}_k$: $\vartheta = \vartheta(\boldsymbol{c}_k)$. The number of thermal degrees of freedom of the

finite element system is denoted by n_ϑ and of the modal system by m_ϑ:

$$\vartheta(\boldsymbol{c}_k) = \boldsymbol{\Phi}_\vartheta(\boldsymbol{c}_k)\, \boldsymbol{z}_\vartheta \,, \qquad 1 \leq k \leq n_\vartheta \,, \tag{26a}$$

$$\boldsymbol{\Phi}_\vartheta(\boldsymbol{c}_k) = [\, \dots \; \vartheta_i \; \dots \,] \,, \qquad 1 \leq i \leq m_\vartheta \,. \tag{26b}$$

The temperatures of all nodes k, assigned to a specific mode i constitute one modal temperature field $\boldsymbol{\vartheta}_i$ and one column of the thermal modal matrix $\hat{\boldsymbol{\Phi}}_\vartheta$ in the finite element discretisation[1]:

$$\boldsymbol{\vartheta}_i = (\, \dots \vartheta_k \dots \,)^T \,, \qquad \boldsymbol{\vartheta}_i \in \mathbb{R}^{n_\vartheta} \,, \tag{26c}$$

$$\hat{\boldsymbol{\Phi}}_\vartheta = [\, \dots \; \boldsymbol{\vartheta}_i \; \dots \,] \qquad \hat{\boldsymbol{\Phi}}_\vartheta \in \mathbb{R}^{n_\vartheta, m_\vartheta} \,. \tag{26d}$$

Hence, each vector $\boldsymbol{\vartheta}_i$ represents a discrete thermal mode, i.e. assigns one temperature to each node or finite element degree of freedom respectively. A mode may be e.g. a solution of the thermal eigenvalue problem $[\hat{\boldsymbol{C}}_{\vartheta\vartheta}\kappa_i + \hat{\boldsymbol{K}}_{\vartheta\vartheta}]\boldsymbol{\vartheta}_i = 0$. Fig. 5 visualises three thermal eigenvectors of the sample structure by colour. The selection of specific modes may also be motivated by given load distributions, as it is demonstrated in Sec. 4.

The following modal reduction of the finite element equations is a standard reduction approach and yields the matrices of the thermal system according to (13):

$$\boldsymbol{C}_{\vartheta\vartheta} = \hat{\boldsymbol{\Phi}}_\vartheta^T \hat{\boldsymbol{C}}_{\vartheta\vartheta}\, \hat{\boldsymbol{\Phi}}_\vartheta \,, \qquad \boldsymbol{K}_{\vartheta\vartheta} = \hat{\boldsymbol{\Phi}}_\vartheta^T \hat{\boldsymbol{K}}_{\vartheta\vartheta}\, \hat{\boldsymbol{\Phi}}_\vartheta \,. \tag{26e}$$

2. The second step consists of a static analysis of the mechanical system. Each thermal mode $\boldsymbol{\vartheta}_i$ constitutes one mechanical load vector $\hat{\boldsymbol{h}}_i$ and results in one corresponding static displacement solution $\boldsymbol{u}_i$, further on called a *thermal response mode*:

$$\hat{\boldsymbol{h}}_i = \boldsymbol{f}(\boldsymbol{\vartheta}_i) \,, \qquad \hat{\boldsymbol{K}}_{uu}\boldsymbol{u}_i = \hat{\boldsymbol{h}}_i \,, \qquad \boldsymbol{u}_i \in \mathbb{R}^{n_u} \,. \tag{27}$$

Fig. 5 shows the thermal response modes by the deformed mesh compared to the undeformed outer circle contour. Since the thermal response modes turned out to be orthogonal regarding the sample structure, a mechanical frequency could be assigned to each thermal response mode.

3. In the third step additional displacement modes have to be evaluated and selected that represent the native mechanical behaviour of the system, see [13] and [14] for appropriate mode selection techniques.

These purely mechanical modes $\boldsymbol{u}_l$ together with the thermal response modes constitute the mechanical modal matrix $\hat{\boldsymbol{\Phi}}_u$ in finite element discretised form:

$$\hat{\boldsymbol{\Phi}}_u = [\, \dots \; \boldsymbol{u}_i \; \dots \; \boldsymbol{u}_l \; \dots] \,, \qquad m_\vartheta < l \leq m_u \,, \qquad \hat{\boldsymbol{\Phi}}_u \in \mathbb{R}^{n_u, m_u} \,. \tag{28a}$$

If the column vectors of $\hat{\boldsymbol{\Phi}}_u$ are linearly dependent, a maximum subset of linearly independent column vectors is selected to meet the demands of the Ritz approach.

[1] The accent ($\hat{}$) indicates finite element quantities if they might be mixed up with the corresponding modal terms.

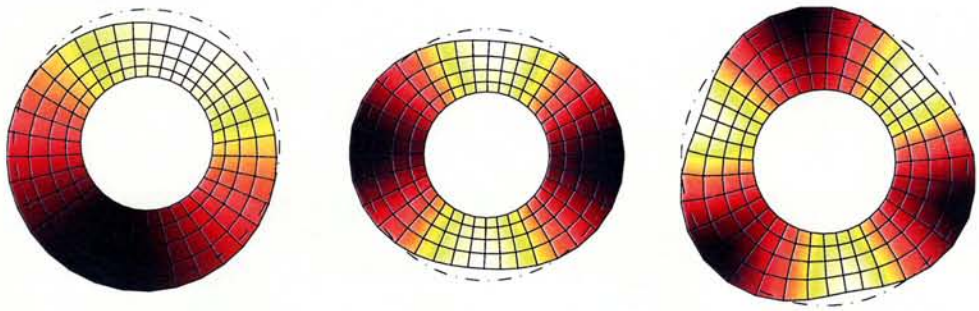

Mode 2
$\kappa_2 = -0.0010$ 1/s
$\bar{\omega}_2 = 18740$ Hz

Mode 4
$\kappa_4 = -0.0038$ 1/s
$\bar{\omega}_4 = 21340$ Hz

Mode 6
$\kappa_6 = -0.0081$ 1/s
$\bar{\omega}_6 = 25230$ Hz

Figure 5: Thermal modes and thermal eigenvalues κ_i, thermal response modes and associated mechanical frequencies $\bar{\omega}_i$ of the sample structure in Fig. 4.

4. The definition (28a) enables the transformation of the mechanical system from the finite element to the multibody description that is based on the modal approach. The modal reduction of the finite element mass and stiffness matrix, $\hat{\boldsymbol{M}}_{uu}$ and $\hat{\boldsymbol{K}}_{uu}$, exemplifies this transformation, which is presented in detail in [8, Ch. 6]

$$\boldsymbol{M}_{uu} = \hat{\boldsymbol{\Phi}}_u^T \hat{\boldsymbol{M}}_{uu} \hat{\boldsymbol{\Phi}}_u \,, \qquad \boldsymbol{K}_{uu} = \hat{\boldsymbol{\Phi}}_u^T \hat{\boldsymbol{K}}_{uu} \hat{\boldsymbol{\Phi}}_u \,. \tag{28b}$$

The load vectors $\hat{\boldsymbol{h}}_i$ describe the influence of the thermal modes on the displacement field. Therefore the thermal-mechanical coupling matrix $\boldsymbol{K}_{\vartheta u}$ of (9) can be provided as the reorganisation of the thermal load vectors:

$$\boldsymbol{K}_{\vartheta u} = \hat{\boldsymbol{\Phi}}_u^T [\, \ldots \; \hat{\boldsymbol{h}}_i \; \ldots \,] \,. \tag{28c}$$

The crucial step of this scheme is the first one, i.e. the modal reduction of the temperature field. The approach used for this step has to be tailored to the modelling task. If this is accomplished the further Steps 2. to 4. concerning the definition of thermal response modes and the corresponding modal reduction of the mechanical field are straightforward and may even be organised as an automated process. The accuracy or the convergence properties respectively of the modal multifield representation rely on an appropriate thermal field description. On the other hand, a substantial reduction of the number of degrees of freedom may be achieved that way. See [15] for more details on the definition of thermal response modes and some verification examples that demonstrate their application.

4 A MACHINE TOOL WITH THERMOELASTIC DEFORMATIONS

4.1 Motivation

Modern machine tool drives show excellent dynamical properties and allow high accelerations of slides and tool heads. However, for point-to-point working tasks the accumulation of high power inputs near frequently used start and stop positions cannot be avoided for physical reasons. Due to performance losses localised thermal loads may be generated and result in an inhomogeneous temperature field of the machine base or other machine components.

The corresponding inhomogeneous thermal expansion causes tool centre point displacements that are difficult to be measured. In industrial applications these thermally induced

displacements are either accepted to be unavoidable or costly cooling devices are designed to ensure a homogeneous thermal state of the machine. However, with increasing demands on the economic efficiency and the accuracy there is a necessity for smart, mechatronic concepts to handle this problem for future generations of high accuracy machine tools.

As a first step towards such a mechatronic concept, an industrial multibody simulation environment has been is extended to deal with the thermoelastic deformation of machine tools. Therefore, the methodological base is provided to develop new measurement and control strategies that account for thermally induced displacements.

4.2 Simulation Scenario

The feasibility study was defined in cooperation with an industrial partner who provided a finite element model of the machine base. The welded construction of the machine is sketched in the SIMPACK model in Fig. 6.

The machine is symmetric w.r.t. a vertical plane and is assembled with two cantilever arms, one at each side. Each cantilever arm is driven by a linear induction device and moves along a magnet liner which is parallel to the y-axis of the machine. The cantilever carries x- and z-drives and the tool head with the tool centre point (TCP) at its tip. The flat workpiece on the machine table in Fig. 6 demonstrates the position of the work-plane.

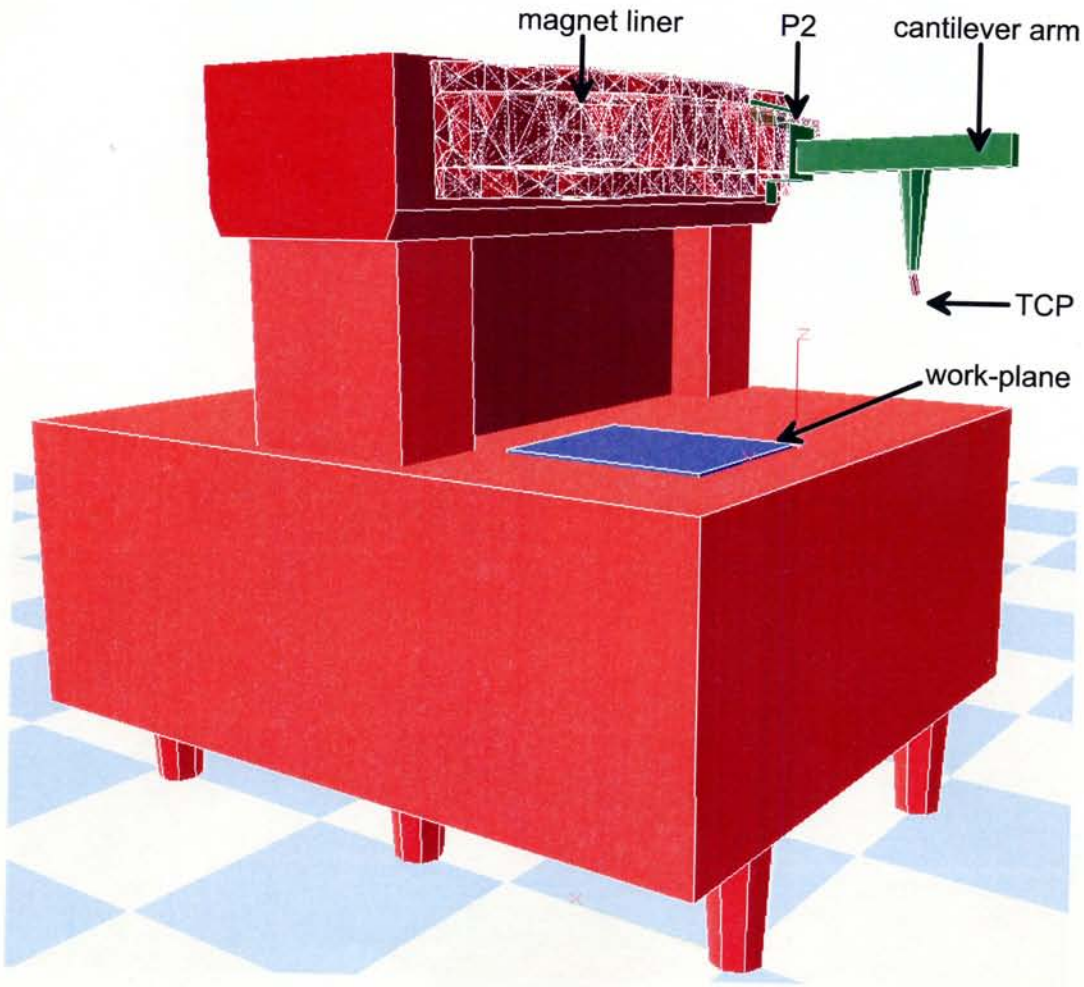

Figure 6: Principle lay-out of the machine tool in SIMPACK.

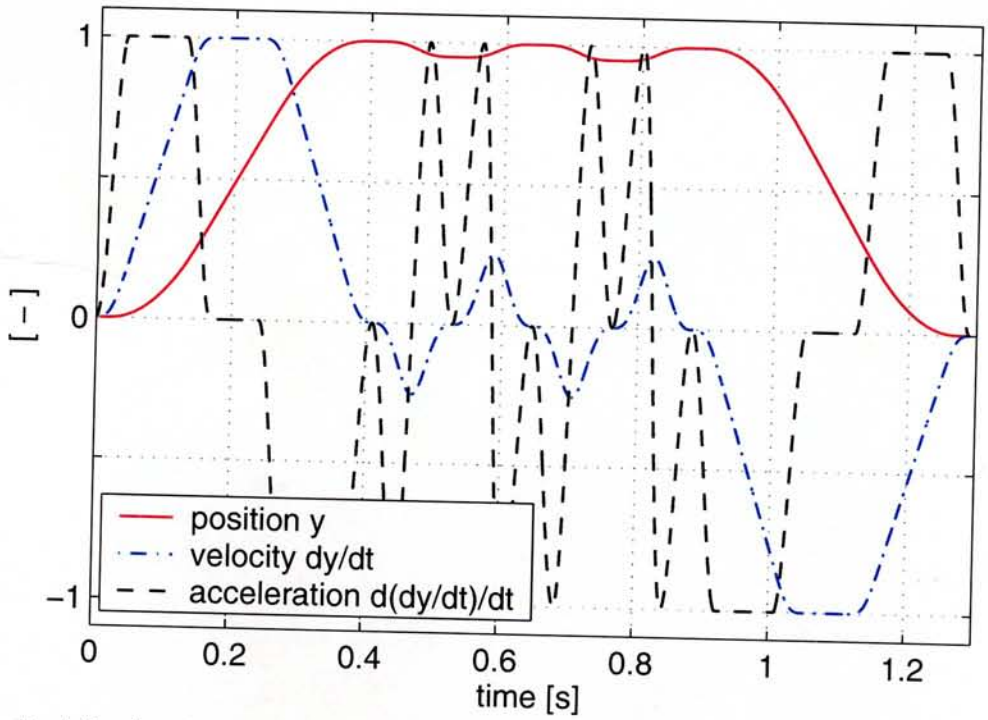

Figure 7: Predefined positioning loop $\bar{y} = \bar{y}(t)$ and its time derivatives in normalised representation.

This study is based on the assumption that the working task of the machine is repeated very often and varies periodically. The objective of the study is to reproduce a constant thermal operating state of the machine that is reached after a sufficiently large time span. This is a frequently observed operating condition in the industrial use of machine tools.

Fig. 7 shows the positioning loop of the cantilever arm along the y-axis that was predefined and taken as the starting point of the feasibility study.

In order to model the thermal behaviour, a heat source of intensity $\bar{q}$ at the position $\bar{y} = \bar{y}(t)$ is considered to move along an isotropic one-dimensional continuum, described by the co-ordinate y. For mathematical representation, the formulation of a point source by means of the Dirac function $\mathfrak{d}(y - \bar{y})$, see [1, (19.28)], is extended by a term that accounts for the geometrical dimensions of the heat source, i.e. the drive head on the cantilever arm. The heat flux is assumed to be distributed as a Gaussian bell-shaped curve with a parameter a that reflects the length of the drive head:

$$-\Lambda\vartheta_{,yy} + \varrho c\dot{\vartheta} = Q(t,y,\bar{y}) = \begin{cases} \bar{q}\,\mathfrak{d}(y-\bar{y}) & \text{point source,} \\ \bar{q}\,\sqrt{\frac{a}{\pi}}\,\exp(-a(y-\bar{y})^2) & \text{distributed source.} \end{cases} \tag{29}$$

For stationary hot running conditions the time dependent terms in (29) have to vanish. The localised heat supply $q = q(y)$ is obtained as time average over one positioning loop with period T:

$$\left.\begin{array}{rcl} \bar{q}(t) & = & \bar{q}(t+nT) \\ \bar{y}(t) & = & \bar{y}(t+nT) \\ n & \to & \infty \end{array}\right\} \Longrightarrow -\Lambda\vartheta_{,yy} \approx \frac{1}{T}\int_0^T Q(t,y,\bar{y})\,\mathrm{d}t = q(y)\,. \tag{30}$$

Since the specific design of the cantilever suspension involves only very small frictional forces, the mechanical power is almost completely invested into the kinetic energy of the

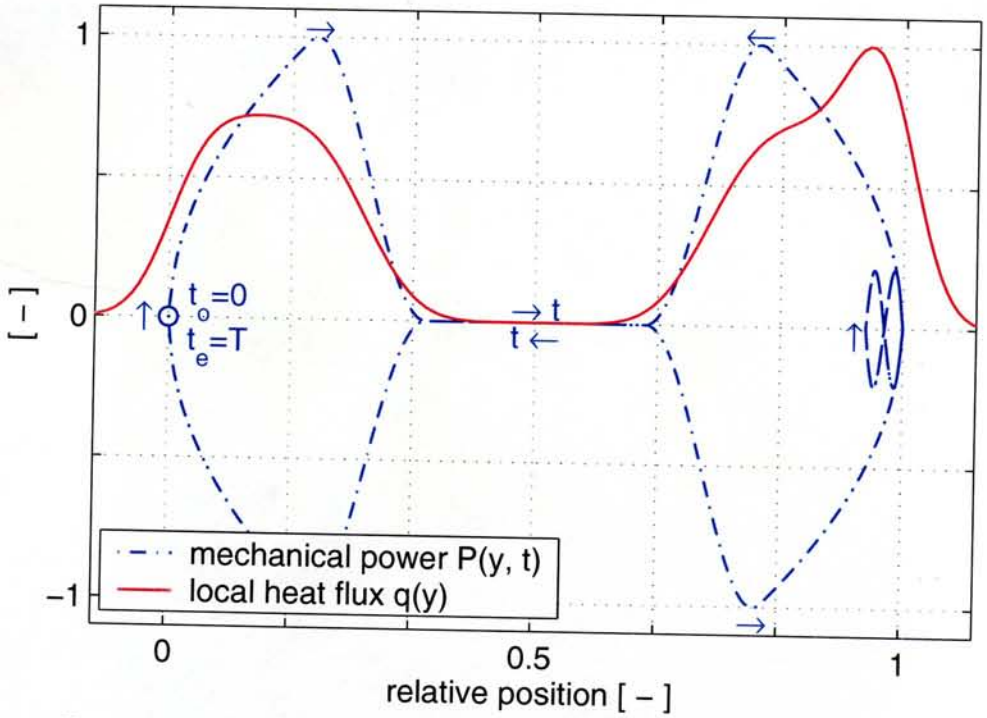

Figure 8: Mechanical power consumption and quasi-stationary heat flux.

cantilever arm and may be easily described based on the predefined kinematic scenario in Fig. 7. If it is assumed, that a constant share of the consumed electrical power is transformed into heat energy and conducted to the surface of the machine base. Then, the localised heat supply $q = q(y)$ is completely defined by (30).

Fig. 8 presents the mechanical power consumption versus the relative position of the cantilever arm on the magnet liner with the time as curve parameter. The start and stop positions are denoted by the relative position 0 and 1 respectively.

The power consumption, specified by the instantaneous product of mass m, velocity $\dot{\tilde{y}}$ and acceleration $\ddot{\tilde{y}}$ from Fig. 7, has distinct maxima in the neighbourhood of start and stop positions. Therefore, the quasi-stationary heat flux accumulates at specific positions on the magnet liner. On the other hand, there are no heat loads at those parts of the magnet liner at which the cantilever arm moves with constant velocity.

4.3 Finite Element Analysis

The thermal finite element model of the machine base consists of 20 641 tetrahedral shaped elements of type Solid90 [16] with 40 471 nodes or thermal degrees of freedom respectively.

A steady state heat transfer FE analysis has been performed using the analytical heat source introduced above as quasi-stationary load. The solid curve in Fig. 8 is taken as heat flux distribution in y-direction along the upper surface of the magnet liner, which is visualised in Fig. 9. In the ξ-direction on the upper surface, the heat flux is modelled to be constant. Robin boundary conditions are defined on the complete surface of the machine base with two different film coefficients to reflect different cooling conditions due to the air-stream forced by the moving cantilever.

The heat transfer analysis is performed separately for each cantilever drive at both sides of the machine. Since the thermal as well as the subsequent mechanical structural

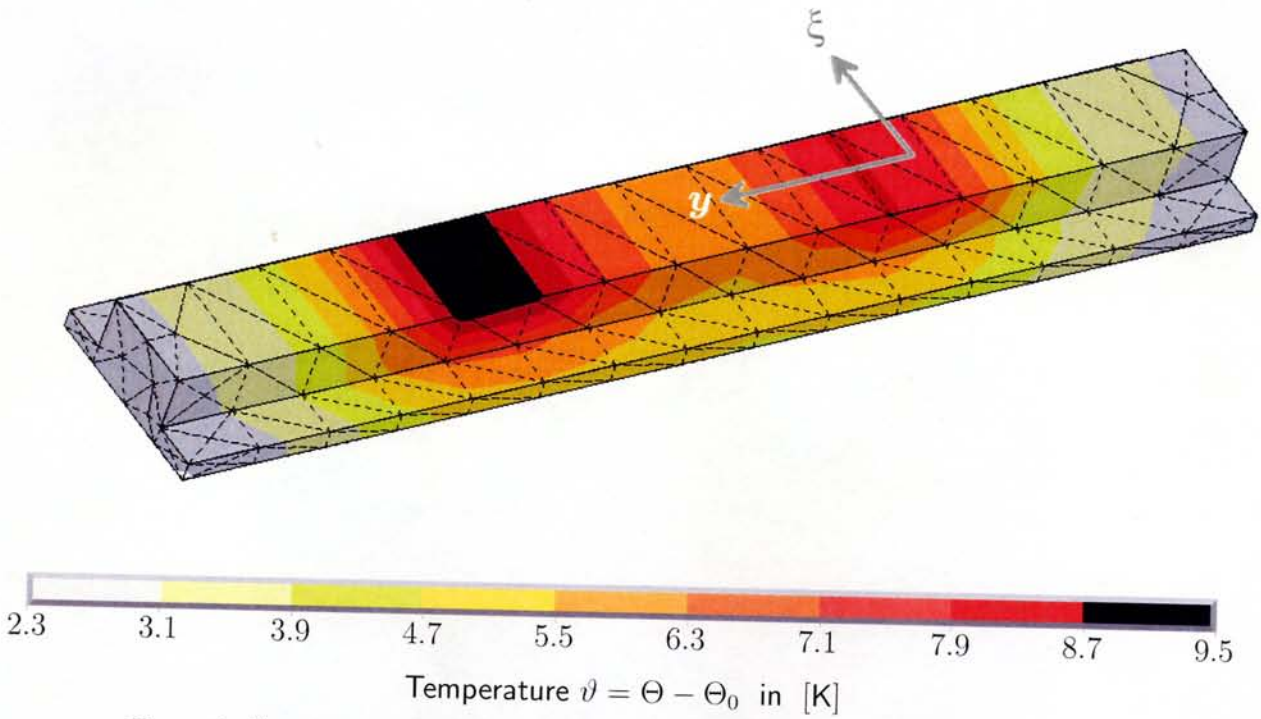

Figure 9: Temperature field at the magnet liner, obtained by finite element analysis.

analysis are linear, the solutions may be superimposed. That way the model definition is open to consider any linear load combination caused by the two cantilever drives. For ease of interpretation the results to present from now on refer to a single load scenario, i.e. the second cantilever drive on the backside of the machine is assumed to be out of use.

Fig. 9 presents the results of one heat transfer FE analysis. Since the temperatures mainly vary on the magnet liner while the other elements of the machine base show only small temperature differences, Fig. 9 only visualises the temperature field of the magnet liner. Two distinct temperature maxima on the magnet liner are clearly visible.

The two FE temperature field solutions of the complete machine base have been applied as separate thermal loads on the mechanical finite element model of the base structure, which uses the same mesh as the thermal FE-model. However, the mesh now specifies 20 641 elements of type Solid95 [16] with 121 413 mechanical degrees of freedom. The solutions of these steady state FE analysis yield the displacement fields of the machine base caused by the temperature fields and are interpreted as thermal response modes according to Sec. 3.3.

Fig. 10 plots the thermal displacements of a reference point on the deformed surface of the magnet liner, which moves along the motion path of the cantilever arm with constant velocity from its start to its stop position. The FE results along the motion path are compared with the corresponding multibody deformations modelled by thermal response modes.

In addition to the steady state analysis, a finite element eigenvalue analysis is performed and 27 eigenmodes of the machine base are obtained. That way, the dynamical properties of the mechanical structure up to the frequency of 400 Hz are considered.

A unified set of modes consisting of 27 mechanical eigenmodes and two thermal response modes has been used to reduce the finite element description of the machine base and get a modal multifield representation according to Sec. 3.3. Eigenmodes and thermal response

modes are only weakly coupled, but the unified set of modes is not orthogonal with respect to the mass and the stiffness matrix. In view of the fact that both groups of modes contain a different physical information which is worth to be retained, the unified set of modes has not been orthogonalised for the multibody simulation.

On a trial basis a supplementary orthogonalisation of the 29 modes has been performed yielding 1 694 Hz and 2 368 Hz as additional frequencies due to the thermal response modes.

4.4 Multibody Simulation

Fig. 6 shows the principle structure of the multibody model and the FE mesh of the magnet liner. Also the complete machine base originates from the FE model and is mechanically represented as flexible body in modal representation.

Since the machine base rests on six feet, which are not fixed to the foundation, its reference frame has three degrees of freedom that allow a plane motion of the machine base frame w.r.t the inertial frame. Six stick-slip force elements reflect the dry friction conditions between machine base and ground.

The suspension of the cantilever arm is modelled by spring-damper elements, which connect the deformed magnet liner and the base of the cantilever arm. The cantilever arm itself is assumed to be rigid. Since the arm moves along the liner, so called *moved markers* [17] have been defined that represent the working points of the suspension forces at the machine base. A moved marker is used as well to model the reference point for Fig. 10.

In order to simulate the working task of the machine tool a controller for the y-drive is modelled. The kinematic scenario from Fig. 7 serves as target specification of the

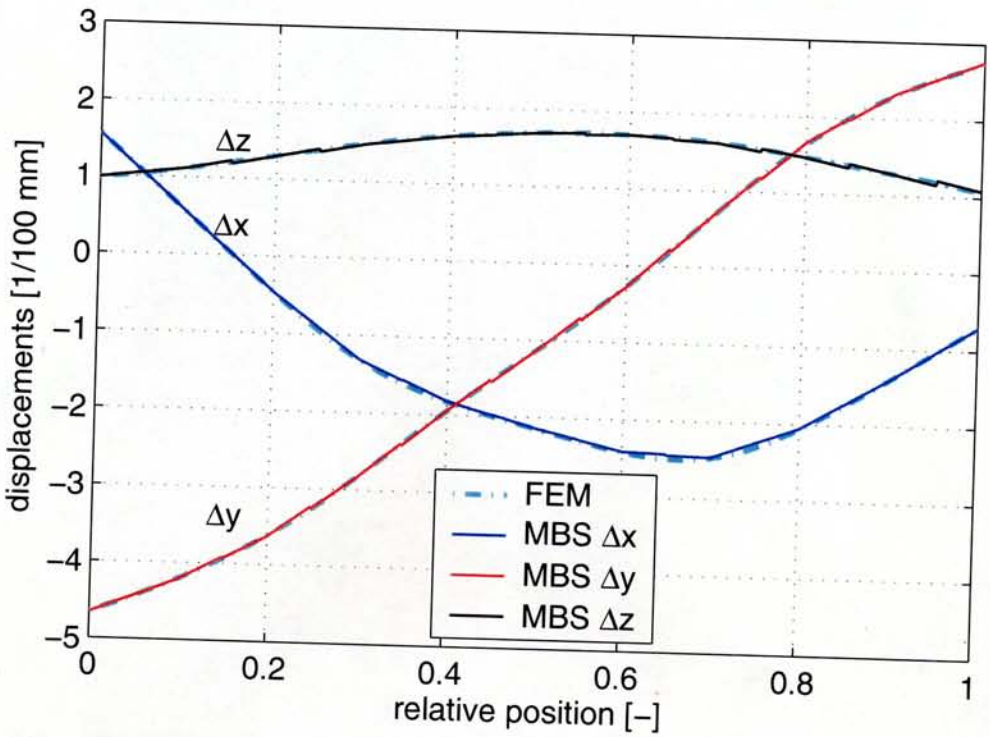

Figure 10: Kinematic comparison of the thermal displacements as evaluated by FEM and the corresponding thermal response mode used for multibody simulation (MBS).

control loop, which is adjusted in such a way that the positioning error induced by the drive control is at least one order of magnitude smaller than the other displacements and cannot falsify the results.

In Fig. 11 three different measurements are compared, where all results concern the displacements w.r.t. the workpiece on the table of the machine tool.

The dotted curves give the tool centre point (TCP) displacements of a multibody simulation without any thermal loads and serve as a reference. These displacements are only caused by the response of the machine base structure and the cantilever suspension to the dynamical loads given by the predefined kinematic scenario.

The other two measurement types in Fig. 11 additionally involve the displacements which are induced by the temperature field of the machine base.

The dashed curves plot the displacements of the reference point P2 on the magnet liner, which moves with the cantilever arm. The solid curves again give the displacements of the TCP at the tip of the cantilever arm. The difference between the P2- and TCP-displacements are caused by the kinematic amplification of the cantilever arm.

The thermally induced displacements influence the motion of the TCP mostly in the neighbourhood of the start position at the beginning and at the end of the simulation. However, since the working task consists of a point-to-point job, these deviations are not crucial in this case. More important are the deflections at the stop position, which is reached several times in the time interval between 0.4 s and 0.9 s. The dotted and the

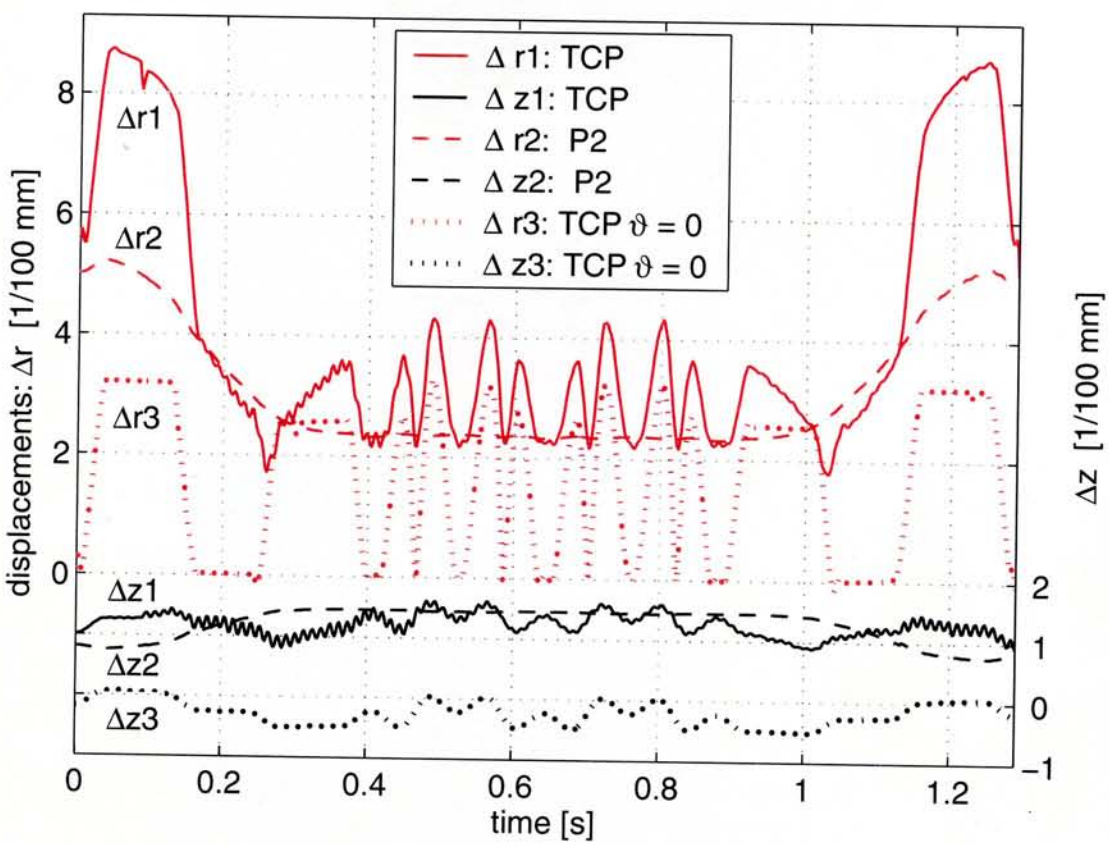

Figure 11: MBS displacement results at the tool center point (TCP) in solid lines and at the reference point P2 on the magnet liner in dashed lines. $\Delta r_{...}$ denotes the absolute displacement parallel to the work plane, while $\Delta z_{...}$ is measured normal to the work-plane. The third couple of curves in dotted lines visualises the TCP-displacements in a simulation without any thermal loads ($\vartheta = 0$).

solid curves differ here by about 10 μm to 20 μm, which is a relevant error concerning the accuracy requirements of machine tools.

Besides the thermal deflection, the response of the machine base structure corresponds mainly to the acceleration curve in Fig. 7 and is of static nature. The vibrations in Fig. 11 primarily originate from the compliance of the cantilever suspension. This statement could be verified by an accompanying simulation, for which the compliance of the cantilever suspension is neglected. The structural damping of the machine base has also no significant influence (Lehr's damping coefficient $d = 0.004$).

The time integration has spent 3 580 CPU-s on a HP 9000/785 workstation with 3 GB memory. This high computational effort is caused by the high frequency band width of the MBS model. Since the inertia terms that correspond to the thermal response modes have not been neglected for this simulation, frequencies up to 2.400 Hz are present, which leads to a very stiff system, cf. [18].

5 CONCLUSIONS AND OUTLOOK

The approximately 160 000 degrees of freedom that are defined by the finite element model of the machine base have been reduced to only 29 degrees of freedom in order to simulate the working task of the machine tool. This modal multifield representation of the structure is therefore suited for controller design as well.

Temperature sensors may be used to observe the thermal state of the real machine base. This thermal state drives the thermal displacement state. With a discretisation by appropriate thermal response modes, it is possible to compensate the thermal displacements by the control law. Thus, the feasibility of the approach which provides a method to improve the accuracy of the machine is demonstrated.

The upgrade of the specific machine tool model from Sec. 4 will include the development of an appropriate approach to discretise the temperature distribution on the magnet liner in space in order to deal with continuously varying working tasks. The transient temperature behaviour of the machine base during the warm-up phase is another point of interest.

Neglecting the inertia terms that correspond to the thermal induced deflections is not only useful to justify the definition of thermal response modes but also improves the numerical properties of a thermoelastic multibody system. Therefore, the consistent transfer of the modal multifield approach into an industrial multibody simulation environment has to exploit this fact and neglect specific mass terms associated to thermal response modes. The discretised equations of motion are then treated as differential algebraic equations (DAE) in a way which was already proposed by SACHAU [19] in order to process modes related to very high stiffness values.

As a final conclusion it may be stated that the presented low-dimensional representation of the distributed phenomenon thermoelasticity opens new chances for system dynamical engineering issues. Complex applications, which could be analysed so far either in detail using the finite element method or only roughly neglecting important influences, may now be modelled more comprehensively from a system dynamical point of view.

REFERENCES

[1] J.L.H. Nowinski. *Theory of thermoelasticity with applications.* Sijthof & Noordhoff International Publishers B.V., Alphen aan den Rijn, Netherlands, 1978.

[2] B. Schweizer and J. Wauer. Atomistic explanation of the Gough-Joule-effect. *The European Physical Journal, B23*, pages 383–390, 2001.

[3] O.C. Zienkiewicz and R.L. Taylor. *The Finite Element Method.* Butterworth Heinemann, Oxford, 5th edition, 2000.

[4] H.J. Bathe. *Finite Element Procedures.* Prentice Hall, New Jersey, 1996.

[5] M.A. Biot. *Variational Principles in Heat Transfer.* Oxford University Press, Oxford, UK, 1970.

[6] A.A. Shabana. *Dynamics of Multibody Systems.* Cambridge University Press, Cambridge, 2nd edition, 1998.

[7] B.A. Boley and J.H. Weiner. *Theory of Thermal Stresses.* Dover Publications, Mineola, New York, 1997.

[8] R. Schwertassek and O. Wallrapp. *Dynamik flexibler Mehrkörpersysteme.* Vieweg Verlag, Braunschweig, 1999.

[9] W. Rulka. *Effiziente Simulation mechatronischer Systeme für industrielle Anwendungen.* PhD thesis, Technische Universität Wien, 1998.

[10] W. Schiehlen. Multibody dynamics: Roots and perspectives. *Multibody System Dynamics*, 1:149–188, 1997.

[11] R. Lifshitz and M.L. Roukes. Thermoelastic damping in micro- and nanomechanical systems. *Physical Review B*, 61(8):5600 – 5609, 2000.

[12] H. Bremer. *Dynamik und Regelung mechanischer Systeme.* Teubner–Verlag, Stuttgart, 1988.

[13] R. Schwertassek, O. Wallrapp, and S. v. Dombrowski. Modal representation of stress in flexible multibody simulation. *Nonlinear Dynamics*, 20:381–390, 1999.

[14] S. Dietz. *Vibration and Fatigue Analysis of Vehicle Systems Using Component Modes.* Number 401 in Fortschritts-Berichte VDI Reihe 12. VDI-Verlag, Düsseldorf, 1999.

[15] A. Heckmann. *The Modal Multifield Approach in Multibody Dynamics.* PhD-Thesis, Department of Mechanical Engineering, University of Hannover, 2005.

[16] ANSYS, Inc. ANSYS® *Release 7.1 Theory Reference*, 2003.

[17] SIMPACK *Reference Manual, Release 8.5.* Weßling, Germany, 2002.

[18] B. Simeon. Numerical analysis of flexible multibody systems. *Multibody System Dynamics*, 6:305–325, 2001.

[19] D. Sachau. *Berücksichtigung von flexiblen Körpern und Fügestellen in Mehrkörpersystemen zur Simulation aktiver Raumfahrtstrukturen.* Bericht aus dem Institut A für Mechanik der Universität Stuttgart, Stuttgart, 1996. PhD thesis.